Maximizing surface-enhanced Raman scattering sensitivity of surfactant-free Ag-Fe3O4 nanocomposites through optimization of silver nanoparticle density and magnetic self-assembly

Zhi Yong Bao, Jiyan Dai, Dang Yuan Lei, and Yucheng Wu

Citation: J. Appl. Phys. **114**, 124305 (2013); doi: 10.1063/1.4823732
View online: http://dx.doi.org/10.1063/1.4823732
View Table of Contents: http://jap.aip.org/resource/1/JAPIAU/v114/i12
Published by the AIP Publishing LLC.

Maximizing surface-enhanced Raman scattering sensitivity of surfactant-free Ag-Fe_3O_4 nanocomposites through optimization of silver nanoparticle density and magnetic self-assembly

Zhi Yong Bao,[1] Jiyan Dai,[1] Dang Yuan Lei,[1,a)] and Yucheng Wu[2,a)]
[1]*Department of Applied Physics, The Hong Kong Polytechnic University, Hong Kong, People's Republic of China*
[2]*College of Material Science and Engineering, Hefei University of Technology, Hefei, People's Republic of China*

(Received 6 August 2013; accepted 11 September 2013; published online 25 September 2013)

Magnetic composite nanomaterials consisting of more than two functional constituents have been attracting much research interests due to the realization of multiple functionalities in a single entity. In particular, integration of ferromagnetic oxides and noble metal nanoparticles (NPs) in composites results in simultaneous magnetic activity and optical response where the optical property of the whole system could be modulated by application of an external magnetic field. In this work, we prepared Ag NPs-coated Fe_3O_4 microspheres as a novel surfactant-free surface-enhanced Raman scattering (SERS) substrate through a solid-phase thermal decomposition reaction. The SERS sensitivity of the fabricated nanocomposites is maximized by adjusting the size and density of Ag NPs supported on the Fe_3O_4 microspheres and further increased by magnetic-field-directed self-assembly of the composite substrates, with both effects attributed to the efficient generation of plasmonic near-field "hot" spots. At the optimal conditions, the prepared substrate is capable of detecting rhodamine 6G molecules at a concentration down to 10^{-12} M, thus demonstrating the great potential of using bifunctional nanocomposites as an excellent candidate for ultra-high sensitive Raman spectroscopy and biosensors. We also reveal the underlying mechanisms responsible for the observed SERS enhancements through full-wave numerical simulations. © *2013 AIP Publishing LLC*. [http://dx.doi.org/10.1063/1.4823732]

INTRODUCTION

Recently, magnetic composite nanostructures composed of two or multiple constituents with different functionalities have received a great deal of attention due to the creation of novel properties that cannot be achieved with a single component.[1–6] Among a large variety of magnetic nanocomposites comprised of different constitutes, combination of ferromagnetic materials with noble metals in an arrangement of core-shell configuration is of particular interest because of the resulting simultaneous optical and magnetic response as well as their flexible control through an application of external magnetic fields.[7–18] These bifunctional structures have demonstrated great potential in biosensing and bioimaging applications. For example, biocompatible crescent-shaped composite nanoparticles (NPs) made of multilayered Au/Fe/Ag/Au have been used as efficient surface-enhanced Raman scattering (SERS) nanoprobes for biomolecular imaging with magnetically modulated detection of low-concentration molecules.[7] Coating ferromagnetic Fe_3O_4 microspheres with noble metal NPs such as Au and Ag in an arrangement analogy to planet-satellite configuration is an alternative approach for constructing such bifunctional SERS substrates. A general approach based on using 3-aminopropyltrimethoxysilane as a linker has been proposed to construct diverse multifunctional Fe_3O_4/metal hybrid nanostructures displaying magnetization, with example demonstrations of Au/Pt and Au/Ag NPs supported on the surface of Fe_3O_4 microspheres.[10] Other typical strategies include ultrasonic synthesis method,[11] thermal decomposition,[12] high-temperature hydrolysis[14] and wet-chemical method,[15] etc. From a practical point of view, SERS spectroscopy as a high-sensitivity identification technique of molecules usually has a very strict requirement on the cleanness of the enhancing substrates in order to minimize the interference signals from the substrates themselves such as pre-adsorbed surfactant molecules. However, the aforementioned preparation methods are often solution-based and involve the use of surfactant molecules during multiple reaction steps. Thus, more efforts are needed to simplify the synthesis method and to improve the substrate cleanness. This is the first issue we are attempting to solve in the present work.

The SERS enhancement mechanisms are roughly divided into electromagnetic (EM) and chemical effects.[19] Numerous studies have demonstrated that EM field intensity can be greatly enhanced within the narrow gap between two metal NPs, and hence enormous SERS enhancements can be achieved for molecules locating in the gap area.[20–23] When two metal NPs are brought close to form an aggregated structure, their transition dipoles will couple to each other and their optical near-fields will coherently interfere at the junction site, resulting in the so-called plasmonic "hot" spots with large near-field enhancements. In general, there are several methods to induce NP aggregation, including chemically induced[24,25] and photoinduced effects,[26,27] etc. In magnetic composite nanostructures, application of an external magnetic field can

a)Authors to whom correspondence should be addressed. Electronic addresses: dylei@polyu.edu.hk and zhiyongbao@126.com

be simply used to arrange or concentrate individual structures into controllable aggregation configuration, thus generating a favorable density of "hot" spots for subsequent SERS enhancements.[7] For instance, Au nanorods-decorated silica-Fe_2O_3 microspheres concentrated under a magnetic field increased the density of "hot" spots thereby boosting the SERS detection limit.[28] Magnetically aggregated Fe_3O_4-Au core-shell nanostructures also demonstrated a higher SERS activity than that of conventional Au NPs under the same conditions.[29] Naturally, the size and density of metal NPs supported on individual microspheres largely affect the total number of "hot" spots formed either between neighboring nanoparticles supported on the same microsphere, or between nanoparticles locating within the contact area of two or more microspheres in the aggregated or self-assembled clusters. Therefore, controllable growth and distribution of noble metal NPs on Fe_3O_4 microspheres or on more general magnetic templates is the key to maximizing the SERS sensitivity of such bifunctional composite nanostructures, but has been largely overlooked in previous studies.[7–16,28,29] This is the second critical problem we are attempting to tackle in the present work.

In this paper, based on previous studies, we report on the fabrication of different kinds of Ag NPs-coated Fe_3O_4 microspheres as surfactant-free SERS substrates and maximization of their SERS sensitivity by adjusting silver NP density and using magnetic-field-induced self-assembly. Precise control over the molar ratio of the Ag precursor generated silver NPs of different dimensions and distribution densities. Under magnetic self-assembly arrangement of these composite structures, we demonstrated reliable SERS detection of rhodamine 6G (R6G) molecules at concentration down to 10^{-12} M, revealing an enhancement of SERS sensitivity up to 10^7.

EXPERIMENT

In order to examine the geometry-dependent SERS response of the composite structures, four samples were prepared with different molar ratios of the Ag precursor and Fe_3O_4. Fe_3O_4 magnetite microspheres were synthesized via a solvothermal reaction in which $FeCl_3$ and CH_3COONa were added in ethylene glycol with stirring, followed by adding $HOCH_2CH_2OH$ into the mixture. The detailed experimental procedure can be found in former studies.[30,31] In this experiment, the amount of Fe_3O_4 microspheres was fixed (0.1 g, 0.43 mmol), and four different amounts of CH_3COOAg (0.035 g, 0.21 mmol; 0.07 g, 0.43 mmol; 0.14 g, 0.86 mmol; and 0.28 g, 1.72 mmol) were added, respectively, resulting in molar ratios of Ag and Fe_3O_4 at 1:2, 1:1, 2:1 to 4:1. During the solid-phase thermal decomposition reaction (heating at 300 °C for 1 h), the CH_3COOAg was reduced to Ag forming Ag NPs supported on the surface of Fe_3O_4 microspheres. The four Fe_3O_4@Ag core-shell samples were labeled as FACS-1, FACS-2, FACS-3, and FACS-4, respectively.

Morphological features of the as-produced composite structures were characterized by FESEM, FEI Quanta 200 FEG, and their crystal structures were studied by JEOL 2010 TEM, operated at 200 kV. Optical absorption measurements were carried out on a TU-1901 model UV-visible double-beam spectrophotometer (Beijing Purkinje General Instrument Co., Ltd, China) operated at a resolution of 2 nm. SERS measurements were performed with a confocal microprobe Raman system (LabRam I from Dilor, France) using an Ar ion laser operating at 514 nm wavelength. The excitation laser power was approximately 1mW with a beam diameter of ca. 2 μm. The integration duration was kept at constant of 5 s.

RESULTS AND DISCUSION

Representative SEM and TEM images of the as-obtained Fe_3O_4@Ag core–shell nanostructures on a Si substrate are presented in Fig. 1. We can clearly see from pictures (a) to (d) that the surface coverage rate of Ag NPs on Fe_3O_4 microspheres increases with increase of the molar concentration of Ag^+ ions used in the reaction. This is because more Ag^+ ions reacted with hydroxyl groups on the surface of Fe_3O_4 microspheres, and thus enhancing the yield of Ag atoms. In order to have a quantitative analysis on the size and density of silver NPs, we plotted in histograms the distribution of Ag NP diameters and gap distances (defined as the distance between two neighbouring NPs on the same microsphere) measured from the TEM images (insets in Fig. 1), and Gaussian fittings were used to extract the average diameter and gap distance for each sample (see

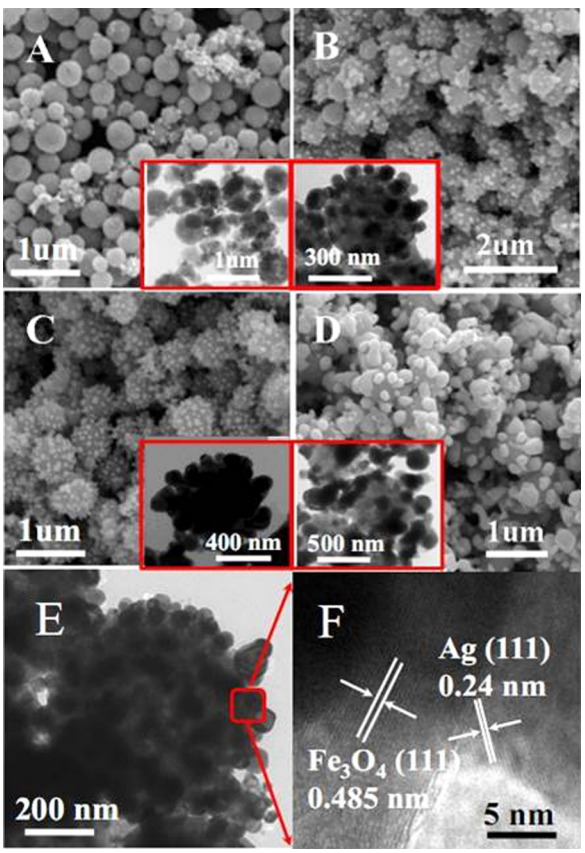

FIG. 1. (A)–(D) SEM images of Fe_3O_4-Ag core-shell structures prepared at different molar concentration ratios of CH3COOAg and Fe_3O_4, 1:2 (A), 1:1 (B), 2:1 (C), and 4:1 (D). Insets are their corresponding TEM images. (E) and (F) High-magnification TEM images showing the attachment of Ag NPs on a Fe_3O_4 microsphere (E) and their lattice constants (F).

Fig. S1).[32] For the molar ratio of 1:2 between Ag and Fe_3O_4, small Ag NPs of about 20 nm diameter are found to distribute on the surface of Fe_3O_4 microspheres with a very low density (see Fig. 1(a)). Increasing the molar ratio of Ag and Fe_3O_4 to 1:1 results in bigger Ag NPs of about 34 nm diameter with an average gap distance of 60 nm, but the NP density is still very low (see Fig. 1(b)). Interestingly, further increase of the molar ratio to 2:1 has little effect on the NP size (36 nm diameter) but significantly increases the density and hence reduces the gap distance to 22 nm (see Fig. 1(c)), which results in a uniform and dense distribution of plasmonic "hot" spots over the microsphere surface. However, such uniform distribution severely degrades when increasing the molar ratio to 4:1, accompanied by an appearance of many large NPs of about 100 nm diameter and 50 nm gap distance (see Fig. 1(d)). This observation is consistent with previous studies that excess Ag^+ ions in the precursor facilitate their aggregation,[33] thus leading to the formation of very large Ag NPs. From the high-magnification TEM images (see Figs. 1(e) and 1(f)), one can clearly observe the uniform attachment of small Ag NPs on the Fe_3O_4 microsphere, and the measured lattice constants correspond to the (111) crystal plane of Ag and Fe_3O_4, respectively. The atomic composition of the prepared Fe_3O_4@Ag core-shell structures was mapped by using X-ray photoelectron spectroscopy (results not shown), from which only Fe, O, Ag, and C elements were observed. This indicates a high purity of the composite nanostructures and hence ensures a reliable SERS detection of the probe Raman molecules.

The optical properties of the Fe_3O_4@Ag core-shell structures were investigated by measuring their absorption spectra in the UV-visible region, with results shown in Fig. 2 for four different samples. The spectrum of bare Fe_3O_4 microspheres is also shown as reference (curve a in Fig. 2), which exhibits no obvious absorption peak. Upon deposition of the Ag-NPs, the composite structures display clear absorption peaks at wavelengths from 392 to 455 nm (curves b, c, d, and e), which belong to the localized surface plasmon resonance (LSPR) of Ag NPs.[34,35] We can see that the LSPR shows a red-shift and broadening with increase of the size and surface coverage of Ag NPs supported on the microspheres. Such red-shift and resonance broadening come from two contributions, including the increased diameter of each individual nanoparticle, which effectively enlarges the plasmonic dipole moment,[36] and the reduced interparticle gap distance, which significantly boosts up the plasmonic coupling strength between two neighbouring nanoparticles.[37]

In Fig. 3, three curves present the hysteresis loops from which we find the magnetization saturation (MS) values for bare Fe_3O_4 microspheres and two Ag-coated Fe_3O_4 composite structures (FACS-2 and FACS-4) to be 53.7, 36.5, and 32.6 emu/g, respectively. The significant decrease of the MS value observed in Fe_3O_4@Ag can be attributed to the diamagnetic contribution of the attached Ag NPs on the surface of the ferromagnetic Fe_3O_4 microspheres.[38] Such excellent magnetic properties indicate that all of the prepared samples have strong magnetic response and can be aggregated or separated easily by applying or removing an external magnetic field.[39]

To test the spectral cleanness of the prepared SERS substrate, we have measured the Raman spectrum of blank Ag NPs-coated Fe_3O_4 microspheres deposited on a Si substrate, with the result shown in Fig. 4(a). Magnetite has five typical Raman bands: two A_{1g} and three E_g.[40] The labelled Raman peaks 384 cm^{-1} and 588 cm^{-1} can be ascribed as two E_g modes[40] while the intense peak observed at 1278 cm^{-1} is assigned to two-magnon scattering of hematite present due to partial oxidation of magnetite.[41] In addition to them, no Raman peaks from any typical surfactant molecules are observed, indicating the high purity of the prepared substrate.

To study the SERS sensitivity of the prepared four structures, we used R6G as the probe molecule. Each sample was immersed in 5 μl R6G aqueous solution at a concentration of 5×10^{-7} M, and then deposited on a glass slide by using a magnetic bar, followed by thorough rinsing with DI water and natural drying in air (see the schematics in Fig. 7). Note that during the drying process, the magnet was moved back and forth along the glass slide, which makes the microspheres assemble in a compact arrangement for the SERS

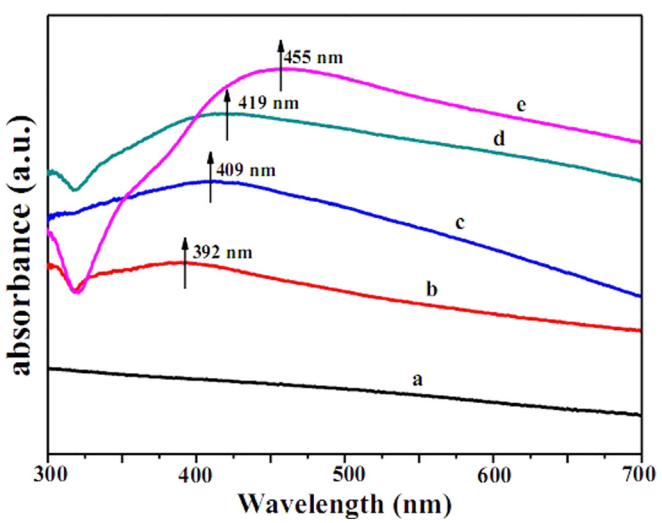

FIG. 2. Absorption spectra of bare Fe_3O_4 (a) and Fe_3O_4-Ag composite structures, FACS-1 (b), FACS-2 (c), FACS-3 (d), and FACS-4 (e).

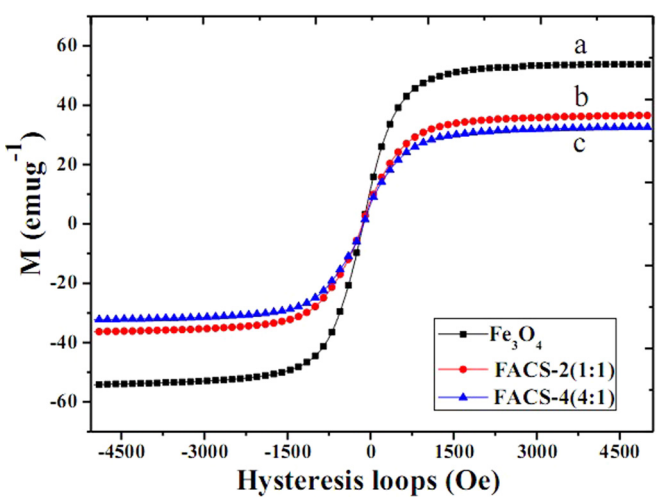

FIG. 3. Magnetic hysteresis loops of bare Fe_3O_4 microspheres (a), FACS-2 (b) and FACS-4 (c) composite structures.

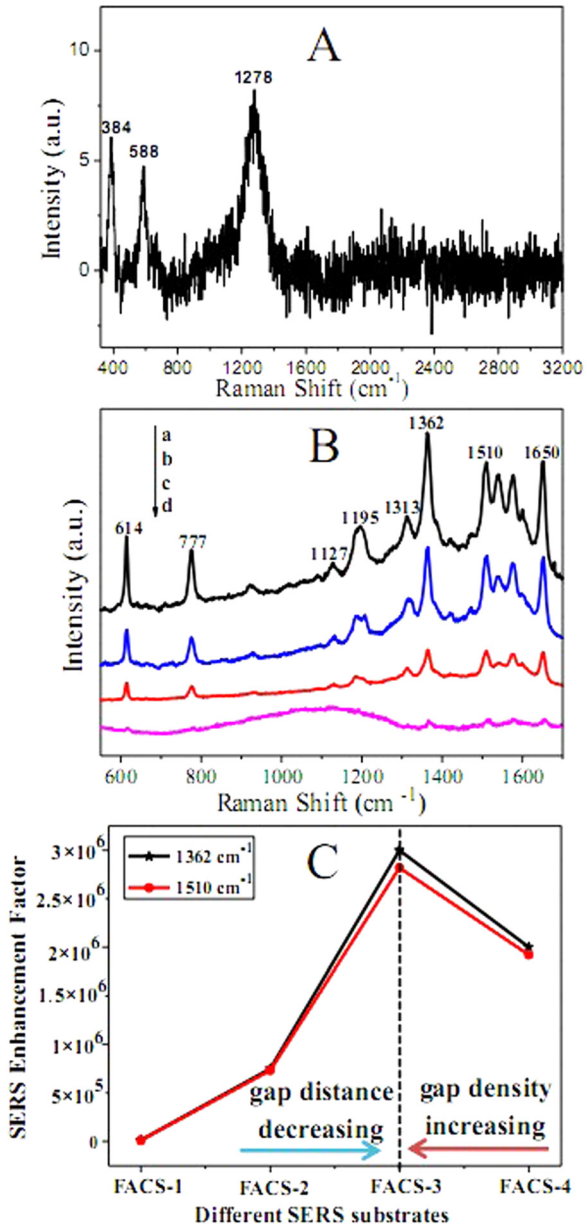

FIG. 4. (A) Raman spectrum collected from pure Ag NPs-coated Fe_3O_4 microspheres. (B) SERS spectra of 5 μl, 5×10^{-7} M R6G molecules adsorbed, respectively, on FACS-3 (curve a), FACS-4 (curve b), FACS-2 (curve c), and FACS-1 (curve d). (C) Calculated EFs for the four different SERS substrates at the 1362 cm^{-1} (asterisk) and 1510 cm^{-1} (circle) bands.

test. Figure 4(b) displays the SERS spectra of R6G molecules collected from the four Fe_3O_4-Ag samples. The characteristic Raman bands of R6G molecules, such as 614, 1362, 1510, and 1650 cm^{-1}, are clearly observed in the spectrum. It is well known that the sharp peaks at 614, 777, and 1127 cm^{-1} are associated, respectively, with C-C-C ring in-plane, out-of-plane, and C-H in-plane vibrations, while the peaks at 1195, 1362, 1510, and 1650 cm^{-1} are assigned to the symmetric modes of in-plane C-C stretching vibrations.[42] We can clearly see from Fig. 4(b) that the SERS signals from FACS-3 (curve a) are much stronger than the others, indicating that the enhanced SERS effect is associated with not only the increase of Ag NP size but also its uniform distribution. The results show that the 1362 cm^{-1} peak intensity from FACS-3 increases by about 1.5- and 4-fold compared to that of FACS-4 and FACS-2, respectively.

From the measured SERS enhancements, we can evaluate the role played by the gap size and density of Ag-NPs in different nanostructures. The Enhancement Factor (EF)[43,44] can be calculated quantitatively according to the following formula:[45–47]

$$EF = (I_{SERS}/N_{SERS})/(I_0/N_0),$$

where I_{SERS} and N_{SERS} are the Raman peak intensity values and the total number of molecules adsorbed on the prepared substrate, and I_0 and N_0 are the corresponding parameters for the control sample (5 μl, 5 mM R6G solution deposited on a Si substrate in our experiment). This calculation is based on the fact that the intensity of the collected SERS signal is proportional to the total number of molecules if the molecules are at a low concentration level. Note that the control experiment was carried out under the same experimental conditions, such as the laser excitation wavelength and illumination power density. The Raman intensity comparison between the control sample and the composite nanostructure FACS-3 is shown in Fig. S2.[32] The calculated EFs for the carbon stretching modes at 1362 cm^{-1} and 1510 cm^{-1} are summarized in Fig. 4(c). It is found that the EF first increases with the molar concentration ratio of Ag precursor and Fe_3O_4 but then decreases, with a maximum value ($\sim 3 \times 10^6$) for FACS-3 (molar ratio 2:1). This trend is consistent with our observation from our distribution of Ag NPs with a moderate size and the smallest gap distance, thereby creating a large number of plasmonic "hot" spots over the whole microsphere surface.

In order to determine the SERS detection limit of the prepared substrates, we have collected the SERS spectra from the FACS-3 sample as a function of the R6G solution concentration (from 10^{-8} to 10^{-12} M), with results shown in Fig. 5. Though the Raman intensity largely decreases with dilution of the R6G solution, we find that the main spectral characteristics of R6G molecules can be still identified even at the solution concentration as low as 10^{-12} M(see the inset of Fig. 5).

We then investigate the effect of magnetic self-assembly of the Ag-coated Fe_3O_4 microspheres on their SERS sensitivity. For this purpose, two samples of FACS-3 with R6G molecules adsorbed were prepared on glass slides, respectively, by normal drop-casting and magnetic-field-induced arrangement. From the comparison between curves a and b in Fig. 6, we can find that the latter substrate shows much stronger SERS signals, with an estimated further enhancement of 3 folds. Such improvement can be attributed to the fact that under application of an external magnetic field, composite microspheres are assembled in an ordered arrangement, which thus increases the number of plasmonic "hot" spots. The results further confirm that assembling the Ag NPs by the magnetic force is an effective method for increasing the sensitivity of SERS substrates. Detailed mechanisms will be discussed in the following.

We now turn to the exploration of the enhancement mechanisms governing the SERS sensitivities observed for the composite structures of different configurations. Ideally,

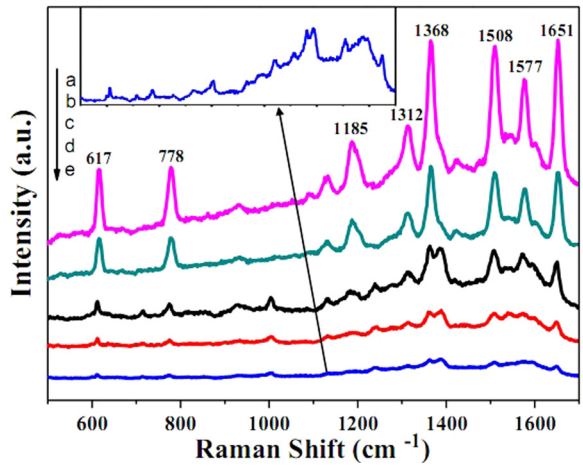

FIG. 5. SERS spectra of R6G molecules of different molar concentrations adsorbed on FACS-3: 10^{-8} M (curve a), 10^{-9} M (curve b), 10^{-10} M (curve c), 10^{-11} M (curve d), and 10^{-12} M (curve e). Insert is a magnified view of curve e.

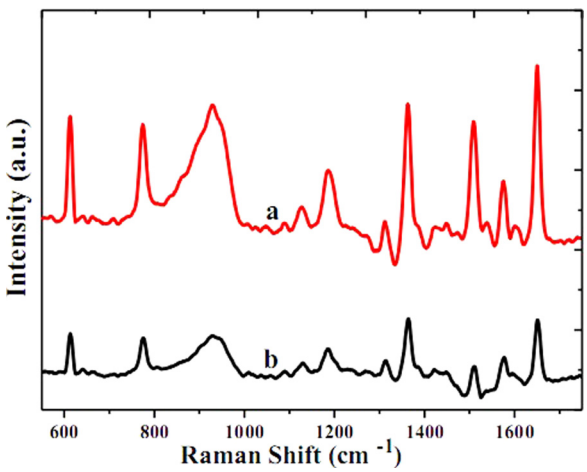

FIG. 6. SERS spectra of 10^{-7} M R6G adsorbed on the FACS-3 substrates prepared by magnetic self-assembly (a) and simple drop-casting (b).

Ag NPs should be closely packed on the surface of Fe_3O_4 microspheres in order to facilitate the formation of plasmonic "hot" spots and increase the surface coverage area. Collective excitation of surface plasmons in the Ag NPs will result in localized strong near-field enhancements, which can subsequently enhance the Raman signals from molecules adsorbed on the NP surface.[48,49] In fact, the four samples investigated in our experiments contain three different types of Ag-NP arrangements, namely isolated small NPs (FACS-1), well-separated moderately sized NPs (FACS-2), closely packed moderately sized NPs (FACS-3) and closely neighbored large NPs (FACS-4). On the one hand, closely packed NPs (FACS-3 and FACS-4) usually exhibit higher near-field enhancements because of the strong plasmonic coupling effect between two NPs and the strong field localization within the gap area.[50–52] Such gaps between the neighboring NPs on the same Fe_3O_4 microsphere create the so-called 1st type "hot" spots as shown in the schematics of Fig. 7. This type of "hot" spots are absent in the structures of FACS-1 and FACS-2 because they contain either isolated small NPs (FACS-1) or well-separated moderately sized NPs (FACS-2), which qualitatively explains their lower SERS EFs (see Fig. 4(b)). Sophisticated numerical simulations are performed to calculate quantitatively the near-field enhancements for the 1st type of "hot" spots in the four samples as we will show later. When the microspheres are arranged in an ordered or closely packed pattern *via* magnetic-field-directed self-assembly, on the other hand, plasmonic "hot" spots can also be created within the gaps formed between the adjacent Ag-NPs attached, respectively, to two different Fe_3O_4 microspheres (see the 2nd type in Fig. 7).[50–52] This gives a qualitative explanation on the observed enhancement of Raman signals from FACS-3 prepared by magnetic self-assembly (see Fig. 6). Because such gaps are usually randomly formed and their gap distances cannot be precisely characterized by SEM or TEM imaging, here we will not examine their effects *via* numerical simulations.

The finite-difference time-domain (FDTD) method[53] was employed to calculate the optical near-field enhancement factors for the 1st type of "hot" spots. The diameter and gap distance of Ag NPs used in the simulations for FACS-2, FACS-3, and FACS-4 were extracted from the TEM imaging (see Fig. 1), and were specified, respectively, as 34 and 60 nm, 36 and 22 nm, and 100 and 50 nm.[32] For the reason of simplicity, we model the neighboring Ag NPs on the same Fe_3O_4 microsphere as NP dimers in a homogeneous environment ($n = 1.33$). This can be justified by the fact that plasmonic near-field coupling dominates over the nearest adjacent nanoparticles. Figures 8(a)–8(c) render the calculated near-field distribution at 514 nm wavelength (corresponding to the laser excitation wavelength) for NP dimers with diameters and gap distances corresponding to FACS-2, FACS-3, and FACS-4, with their spatially averaged field-intensity EFs plotted in Fig. 8(d). We can clearly see that the field intensity is largely enhanced within the dimer gap of FACS-3 (36 nm diameter and 22 nm gap distance) compared to the other two structures

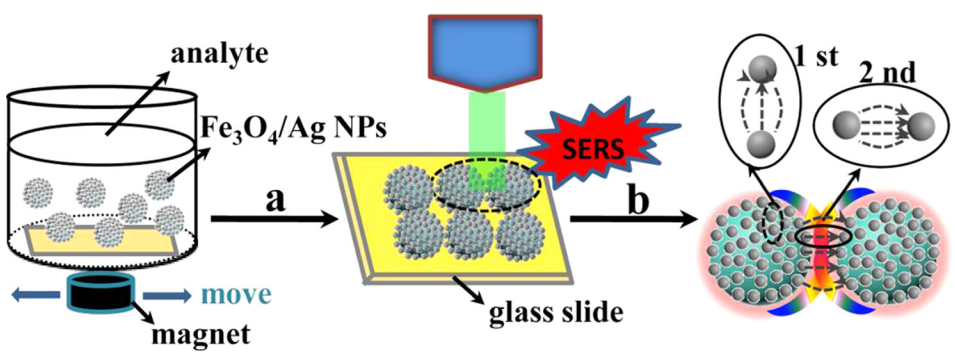

FIG. 7. (a) Schematic diagrams of the magnetic self-assembly fabrication of Fe_3O_4@Ag SERS substrates. (b) Two types of plasmonic "hot" spots formed between Ag-NPs. The 1st type stands for the gaps between Ag-NPs located on the same Fe_3O_4 microsphere while the 2nd type refers to the gaps between two Ag-NPs located, respectively, on the surface of two neighboring Fe_3O_4 microspheres.

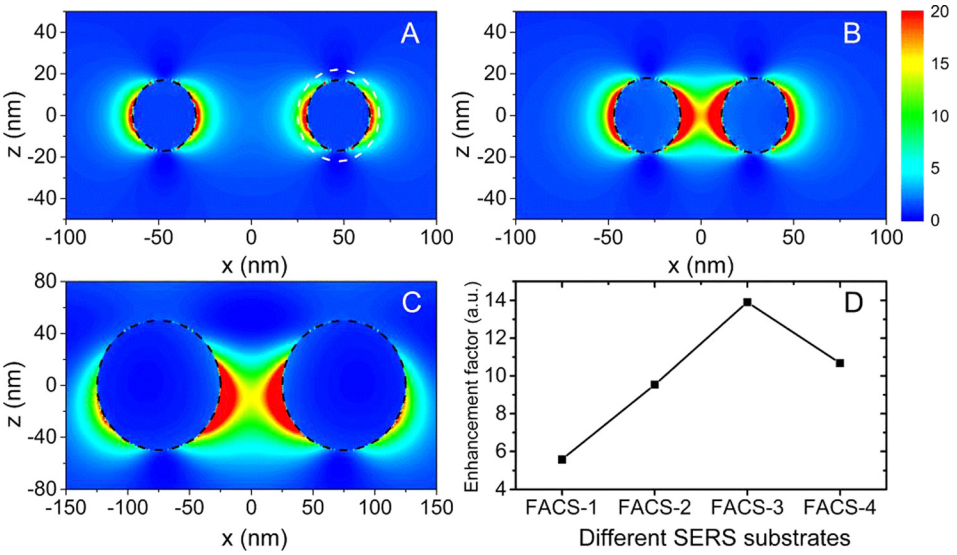

FIG. 8. (A)–(C) Calculated electric-field intensity distribution for Ag NP dimers of different diameters and gap distances, 34 and 60 nm (A), 36 and 22 nm (B), and 100 and 50 nm (C). The dashed black circle indicates the boundary of each sphere. The incident polarization is along the dimer axis connecting the two nanoparticles. (D) Spatially averaged field-intensity enhancement factor for an isolated Ag NP of 20 nm diameter (FACS-1) and the three NP dimers in (A)–(C). Spatial integration of the normalized field intensity was performed within the shell area between the dashed white and black circles ($R < r < R + 5$ with R the radius of each sphere).

because of the smallest gap distance. Spatially averaged field intensity EFs shown in Fig. 8(d) exhibit exactly the same trend as the SERS EFs observed in Fig. 4(c). This indicates that the electromagnetic contribution from closely packed Ag NPs on each Fe_3O_4 microsphere dominates the total SERS response of the substrate, highlighting the importance of flexible control over the metal NP size and density in such bifunctional composite structures.

CONCLUSION

In summary, by adjusting the mole ratio of reactant, we have maximized the SERS sensitivity of such composite structures by controlling the size and density of Ag NPs and magnetically self-assembling the microspheres in an ordered or closely packed arrangement. We have shown that, at the optimal conditions, the prepared substrate is capable of detecting R6G molecules at a concentration as low as 10^{-12} M, revealing a combined SERS enhancement factor exceeding 10^7. The detailed enhancement mechanisms have been discussed by identifying the two types of plasmonic "hot" spots formed in such composite structures, and further verified with numerical simulations.

ACKNOWLEDGMENTS

This work was supported by the National Key Basic Research Program of China (973 Program, 2013CB632900), the National Natural Science Foundation of China (NSFC) (Nos. 91023030 and 51072044), the Specialized Research Fund for the Doctoral Program of Higher Education (No. 20100111110012), and the International Scientific and Technological Cooperation Project of Anhui Province (No. 10080703017). D.Y.L. acknowledges the Grants 1-ZVAL and 1-ZVAW administrated by The Hong Kong Polytechnic University.

[1]B. S. Kim, J. M. Qiu, J. P. Wang, and T. A. Taton, Nano Lett. **5**, 1987–1991 (2005).
[2]G. Wang, Z. Gao, S. Tang, C. Chen, F. Duan, S. Zhao, S. Lin, Y. Feng, L. Zhou, and Y. Qin, ACS Nano **6**, 11009–11017 (2012).
[3]J. Kim, S. Park, J. E. Lee, S. M. Jin, J. H. Lee, I. S. Lee, I. Yang, J. S. Kim, S. K. Kim, M. H. Cho, and T. Hyeon, Angew. Chem., Int. Ed. **45**, 7754–7758 (2006).
[4]M. Hu, A. A. Belik, M. Imura, and Y. Yamauchi, J. Am. Chem. Soc. **135**, 384–391 (2013).
[5]C. Xu and S. Sun, Adv. Drug Delivery Rev. **65**, 732–743 (2013).
[6]B. Santara, B. Pal, and P. K. Giri, J. Appl. Phys. **110**, 114322 (2011).
[7]G. L. Liu, Y. Lu, J. Kim, J. C. Doll, and L. P. Lee, Adv. Mater. **17**, 2683–2688 (2005).
[8]Z. Xu, Y. Hou, and S. Sun, J. Am. Chem. Soc. **129**, 8698–8699 (2007).
[9]M. Y. Sha, H. X. Xu, M. J. Natan, and R. Cromer, J. Am. Chem. Soc. **130**(51), 17214–17215 (2008).
[10]S. J. Guo, S. J. Dong, and E. Wang, Chem. Eur. J. **15**, 2416–2424 (2009).
[11]B. L. Lv, Y. Xu, H. Tian, D. Wu, and Y. H. Sun, J. Solid State Chem. **183**, 2968–2973 (2010).
[12]F. H. Lin, W. Chen, Y. H. Liao, R. A. Doong, and Y. D. Li, Nano Res. **4**, 1223–1232 (2011).
[13]J. K. Lim and S. A. Majetich, Nano Today **8**, 98–113 (2013).
[14]L. Zhang, W. F. Dong, Z. Y. Tang, J. F. Song, H. Xia, and H. B. Sun, Opt. Lett. **35**, 3297–3299 (2010).
[15]H. B. Hu, Z. H. Wang, L. Pan, S. Zhao, and S. Zhu, J. Phys. Chem. C **114**, 7738–7742 (2010).
[16]K. Kim, J. Y. Choi, H. B. Lee, and K. S. Shin, ACS Appl. Mater. Interfaces **2**, 1872–1878 (2010).
[17]Y. Lee, M. A. Garcia, N. A. Frey Huls, and S. Sun, Angew. Chem., Int. Ed. **49**, 1271–1274 (2010).
[18]X. Sun, S. Guo, C.-S. Chung, W. Zhu, and S. Sun, Adv. Mater. **25**, 132–136 (2013).
[19]M. Moskovits, Rev. Mod. Phys. **57**, 783–826 (1985).
[20]S. M. Nie and S. R. Emory, Science **275**, 1102–1106 (1997).
[21]H. X. Xu, E. J. Bjerneld, M. Käll, and L. Börjesson, Phys. Rev. Lett. **83**, 4357–4360 (1999).
[22]G. W. Lu, C. Li, and G. Q. Shi, Chem. Mater. **19**, 3433–3440 (2007).
[23]K. Kneipp, H. Kneipp, I. Itzkan, R. R. Dasari, and M. S. Feld, Chem. Rev. **99**, 2957–2976 (1999).
[24]A. M. Schwartzberg, C. D. Grant, A. Wolcott, C. Talley, C. T. Huser, R. Bogomolni, and J. Z. Zhang, J. Phys. Chem. B **108**, 19191–19197 (2004).
[25]E. Messina, E. Cavallaro, A. Cacciola, M. A. Latì, P. G. Gucciardi, F. Borghese, P. Denti, R. Saija, G. Compagnini, M. Meneghetti, V. Amendola, and O. M. Maragò, ACS Nano **5**, 905–913 (2011).
[26]R. Jin, Y. W. Cao, C. A. Mirkin, K. L. Kelly, G. C. Schatz, and J. G. Zheng, Science **294**, 1901–1903 (2001).
[27]A. Pyatenko, M. Yamaguchi, and M. Suzuki, J. Phys. Chem. C **111**, 7910–7917 (2007).
[28]M. Spuch-Calvar, L. Rodríguez, P. Morales, R. A. Puebla, and L. Marzan, J. Phys. Chem. C **113**, 3373–3377 (2009).
[29]D. A. Wheeler, S. A. Adams, T. L. Luke, A. T. Castro, and J. Z. Zhang, Ann. Phys. **524**, 670–679 (2012).
[30]H. Deng, X. L. Li, Q. Peng, X. Wang, J. P. Chen, and Y. D. Li, Angew. Chem., Int. Ed. **44**, 2782–2785 (2005).

[31]L. B. Yang, Z. Y. Bao, Y. C. Wu, and J. H. Liu, J. Raman Spectrosc. **43**, 848–856 (2012).
[32]See supplementary material at http://dx.doi.org/10.1063/1.4823732 for the detailed determination of the diameter and gap distance of Ag nanoparticles and for the Raman intensity comparison between the control sample and the composite nanostructure.
[33]Q. An, P. Zhang, J. M. Li, W. F. Ma, J. Guo, J. Hu, and C. C. Wang, Nanoscale **4**, 5210–5216 (2012).
[34]H. J. Chen, L. Shao, Q. Li, and J. F. Wang, Chem. Soc. Rev. **42**, 2679–2724 (2013).
[35]K. Kim, H. J. Jang, and K. S. Shin, Analyst **134**, 308–313 (2009).
[36]C. F. Bohren and D. R. Huffman, *Absorption and Scattering of Light by Small Particles* (Wiley, New York, 1998).
[37]N. J. Halas, S. Lal, W. S. Chang, S. Link, and P. Nordlander, Chem. Rev. **111**, 3913–3961 (2011).
[38]Y. Sun, Y. Tian, M. He, Q. Zhao, C. Chen, C. Hu, and Y. Liu, J. Electron. Mater. **41**, 519–523 (2012).
[39]Y. Chi, Q. Yuan, Y. J. Li, J. C. Tu, L. Zhao, N. Li, and X. T. Li, J. Colloid Interface Sci. **383**, 96–102 (2012).
[40]S. W. da Silva, T. F. O. Melo, M. A. G. Soler, E. C. D. Lima, M. F. da Silva, and P. C. Morais, IEEE Trans. Magn. **39**, 2645–2647 (2003).
[41]D. L. A. de Faria, S. V. Silva, and M. T. de Oliveira, J. Raman Spectrosc. **28**, 873–878 (1997).
[42]Z. Q. Tian, B. Ren, and D. Y. Wu, J. Phys. Chem. B **106**, 9463–9483 (2002).
[43]M. Zamuner, D. Talaga, F. Deiss, V. Guieu, A. Kuhn, P. Ugo, and N. Sojic, Adv. Funct. Mater. **19**, 3129–3135 (2009).
[44]P. G. Etchegoin, M. Meyer, E. Blackie, and E. C. Le Ru, Anal. Chem. **79**, 8411–8415 (2007).
[45]X. Li, Y. Zhang, Z. X. Shen, and H. J. Fan, Small **8**, 2548–2554 (2012).
[46]Y. Yang, Z. Y. Li, K. Yamaguchi, M. Tanemura, Z. R. Huang, D. L. Jiang, Y. H. Chen, F. Zhou, and M. Nogami, Nanoscale **4**, 2663–2669 (2012).
[47]E. C. Le Ru, E. Blackie, M. Meyer, and P. G. Etchegoin, J. Phys. Chem. C **111**, 13794–13803 (2007).
[48]B. H. Jun, G. Kim, J. Baek, H. Kang, T. Kim, T. Hyeon, D. H. Jeong, and Y. S. Lee, Phys. Chem. Chem. Phys. **13**, 7298–7303 (2011).
[49]T. You, P. Yin, L. Jiang, X. Lang, L. Guo, and S. Yang, Phys. Chem. Chem. Phys. **14**, 6817–6825 (2012).
[50]D. Y. Lei, A. Aubry, S. A. Maier, and J. B. Pendry, New J. Phys. **12**, 093030 (2010).
[51]A. Aubry, D. Y. Lei, S. A. Maier, and J. B. Pendry, Phys. Rev. Lett. **105**, 233901 (2010).
[52]D. Y. Lei, A. Aubry, S. A. Maier, and J. B. Pendry, ACS Nano **5**, 597–607 (2011).
[53]D. M. Sullivan, *Electromagnetic Simulation Using the FDTD Method* (IEEE Press, Piscataway, 2000).